Research Article

Hongbo Liu*, Rongyuan Xie*, Min Li, Caidong Zhang, Hongyong Yao, Zhiqiang Tian, Haibin Yang, Zhanli Liu, Qiang Wang, and Ju Kang

Analysis of the evolution law of oxide inclusions in U75V heavy rail steel during the LF-RH refining process

https://doi.org/10.1515/htmp-2022-0257 received August 22, 2022; accepted November 30, 2022

Abstract: The number density, size and composition of inclusions in U75V heavy rail steel during ladle furnace (LF)-RH refining process were studied by an Aztec-Feature inclusion automatic software which equipped with a field emission microscope. The results showed that the MnO-SiO₂-Al₂O₃-type inclusions were the main inclusions at LF start. The MnO-SiO₂-Al₂O₃-type inclusions were transformed into the CaO-SiO₂-Al₂O₃-type inclusions during the LF refining process because of the Ca and Al elements which were brought by ferroalloy. At the RH start stage, the main inclusions were CaO-SiO₂-Al₂O₃-type inclusions with low melting temperature and CaO-MgO-Al₂O₃-type inclusions with high melting temperature in the sample. And, the CaO-MgO-Al₂O₃-type inclusions were obviously removed during RH vacuum treatment. The average compositions of CaO-SiO₂-Al₂O₃-type inclusions had no obvious change from RH vacuum holding for 15 min, RH vacuum break to RH soft blowing.

Ju Kang: Beijing Key Laboratory of Pipeline Critical Technology and Equipment for Deepwater Oil & Gas Development, Beijing Institute of Petrochemical Technology, Beijing, 102617, China

Keywords: U75V heavy rail steel, $LF \rightarrow RH$ refining process, oxide inclusions, evolution law, Inclusion automatic scanning

1 Introduction

Due to the particularity of service conditions, heavy rail steel is required to have high purity [1–3]. In the smelting process of the heavy rail steel, silicon manganese or silicon calcium barium alloys with very low aluminum content are generally added after converter or in the ladle furnace (LF) refining process for deoxidation [4-6]. Nowadays, the content of total oxygen (TO) in heavy rail steel billets can be controlled below 10 ppm [7]. However, a numerical study showed that the large-size oxide inclusions were the main reason inducing the ultrasonic test defects in steel rail. Zhiyong et al. [8] investigated the typical inclusions in heavy rail steel found that the composition in billet is basically the same as in rail, mainly CaO-SiO₂-Al₂O₃-MgO inclusions, with spherical shape and lower melting point, and appears as spherical or branching clusters after rolling. Jianghua et al. [9]. pointed out that there existed a large number of MgO-Al2O3 inclusions with the size of 20-30 µm in the ultrasonic flaw detection samples, which would deteriorate the properties in heavy rail steel. Besides, Yanping et al. [10] suggested that MgO-Al₂O₃ inclusions were easily found in casting bloom, steel rail and tensile fracture, which may be formed inside the submerged nozzle.

In the present work, the composition and quantity of CaO (MnO)–SiO₂–Al₂O₃–MgO oxide inclusions in LF–RH refining in heavy rail steel were systematically investigated through Aztec-Feature automatically scanning of inclusions configured by Zeiss Ultra55 field emission scanning electron microscopy. The study provides an important reference for the effective removal of oxide inclusions in steel and the formulation of reasonable process parameters.

^{*} Corresponding author: Hongbo Liu, Advanced Technology Innovation Center, Materials Technology Research Institute, HBIS Group, Shijiazhuang, Hebei, 050023, China,

e-mail: ustbliuhongbo@163.com

^{*} Corresponding author: Rongyuan Xie, Digital Government Division, HBIS Digital Technology Co., Ltd., Shijiazhuang, Hebei, 050000, China, e-mail: ncepuxierongyuan@163.com Min Li, Zhiqiang Tian, Zhanli Liu, Qiang Wang: Advanced Technology Innovation Center, Materials Technology Research Institute, HBIS Group, Shijiazhuang, Hebei, 050023, China Caidong Zhang, Hongyong Yao: Materials Technology Research Institute, HBIS Group, Shijiazhuang, Hebei, 050023, China Haibin Yang: Handan Steel Company, HBIS Group, Handan, Hebei, 056015, China

2 — Hongbo Liu et al. DE GRUYTER

2 Materials and methods

2.1 Materials

The chemical composition of U75V heavy rail steel in the current study is listed in Table 1. The production route for heavy rail steel was basic oxygen furnace—LF refining—RH vacuum degassing (RH)—continuous casting. The samples used in experiments were mainly obtained in the LF—RH stage and the specific sampling stages are LF start, LF first-time electrode heating, LF second-time electrode heating, RH start, RH vacuum maintaining for 5 min, RH vacuum maintaining for 10 min, RH vacuum maintaining for 15 min, RH breaking and RH soft-blowing ending.

2.2 Methods

The specimens were processed into φ 30 mm \times 18 mm cylindrical sample, and the corresponding surface 5 mm from bottom of the sample was selected as the inclusion observation surface. To ensure the smoothness of the inclusion observation surface, the German ATM automatic grinding machine was used for rough grinding, fine grinding and polishing of each sample. Then, the composition, size and morphology of inclusions of specimens were statistically analyzed by Zeiss Ultra55 field emission scanning electron microscopy, equipped with the Aztec Feature automatic inclusion analysis system. The automatic scanning area was set to 225 mm², and the minimum inclusion size detected was 3 µm to acquire accurate quantitative. However, it is worth noticing that the automatic inclusions scanning area designed in this study is much larger than others. In addition, the contents of TO and nitrogen ([N]) were analyzed by LECO combined nitroxy-hydrogen analyzer.

The results measured by automatic inclusions analysis are converted into the corresponding oxide component, which are projected onto different ternary phase diagrams. According to the composition of the first three main oxide components, the inclusions in heavy rail are classified as MnO–SiO₂–Al₂O₃-, CaO–SiO₂–Al₂O₃- and CaO–MgO–Al₂O₃-type inclusion. The classification criteria are given in Table 2.

3 Results

3.1 Contents of TO and TN

The contents of TO and total nitrogen (TN) in samples during LF–RH refining process are shown in Figure 1. It can be seen that the TO in heavy rail steel decreased significantly from 167 ppm when LF start to 24 ppm after LF first-time electrode heating. Subsequently, with the progress of LF refining, the TO in steel continued to decrease, eventually falling to 11 ppm at the end of LF. During the RH vacuum refining, the TO has no significant change from RH start to RH vacuum maintaining for 10 min whereas T[O] declines from 12 to 7 ppm when the RH vacuum holds for 10–15 min. However, there exists a slight increase at the RH vacuum breaking stage, the reason may be caused by the mixed steel and slag due to the short charging time. Finally, the TO drops from 12 to 7 ppm again after RH soft blowing.

In addition, during the LF process, the content of N increases, which was closely related to the addition of raw materials, electrode loss and secondary oxidation caused by the strong bottom-blowing argon stirring in

Table 1: Main composition of U75V heavy rail steel (wt%)

Element (wt%)	С	Si	Mn	Р	S	Als	٧
Internally controlled standard Contents	0.72-0.80	0.5-0.7	0.8-1.00	≤0.025	≤0.015	≤0.004	0.04-0.07
	0.79	0.62	0.97	0.017	0.004	0.0038	0.056

Table 2: Standard for classification of oxide inclusions in heavy rail steel

Oxide inclusion in heavy rail steel (MnS ≤10 wt%)	MnO > MgO	CaO > MnO	$MnO-SiO_2-Al_2O_3$
		CaO < MnO	$CaO-SiO_2-Al_2O_3$
	MnO < MgO	$SiO_2 > MgO$	$CaO-SiO_2-Al_2O_3$
		$SiO_2 < MgO$	$CaO-MgO-Al_2O_3$

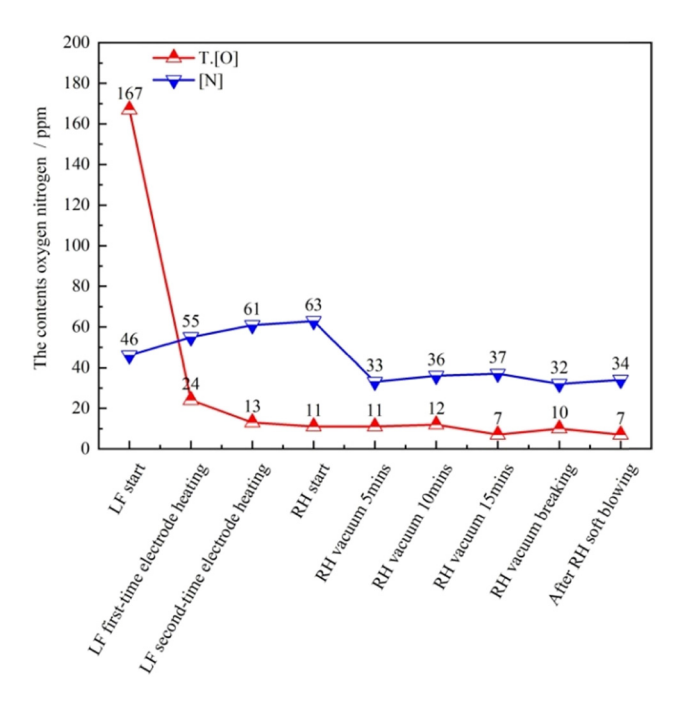


Figure 1: Evolution of contents of TO and TN during LF-RH refining process in heavy rail steel.

the desulfurization process. N can be removed well during the RH refining process, it can be reduced from 63 to 33 ppm in the first 5 min at the RH vacuum stage. After that, it has no obvious changes.

3.2 Morphology and composition of inclusions

The morphology and chemical composition of the main types of inclusions during the LF-RH refining process in heavy rail steel are shown in Figure 2.

As shown in these figures, the main inclusion changes from $MnO-SiO_2-Al_2O_3$ type at the LF start stage to $CaO-SiO_2-Al_2O_3$ type (see Figure 2(b1)) at RH start. It can be seen from Figure 2(b2) that the $CaO-MgO-Al_2O_3$ -type inclusion was also observed at the RH start stage. However, the $CaO-MgO-Al_2O_3$ -type inclusions were rarely found after RH vacuum holding for 10 min. The $CaO-SiO_2-Al_2O_3$ -type inclusions were kept since RH start, and the chemical compositions of which showed little change from RH start to the RH vacuum breaking stage. Furthermore, the element mappings of typical inclusion formed at the vacuum-breaking stage (see Figure 3) verified that the main components were CaO, SiO_2 , and Al_2O_3 , which belonged to the $CaO-SiO_2-Al_2O_3$ -type inclusion.

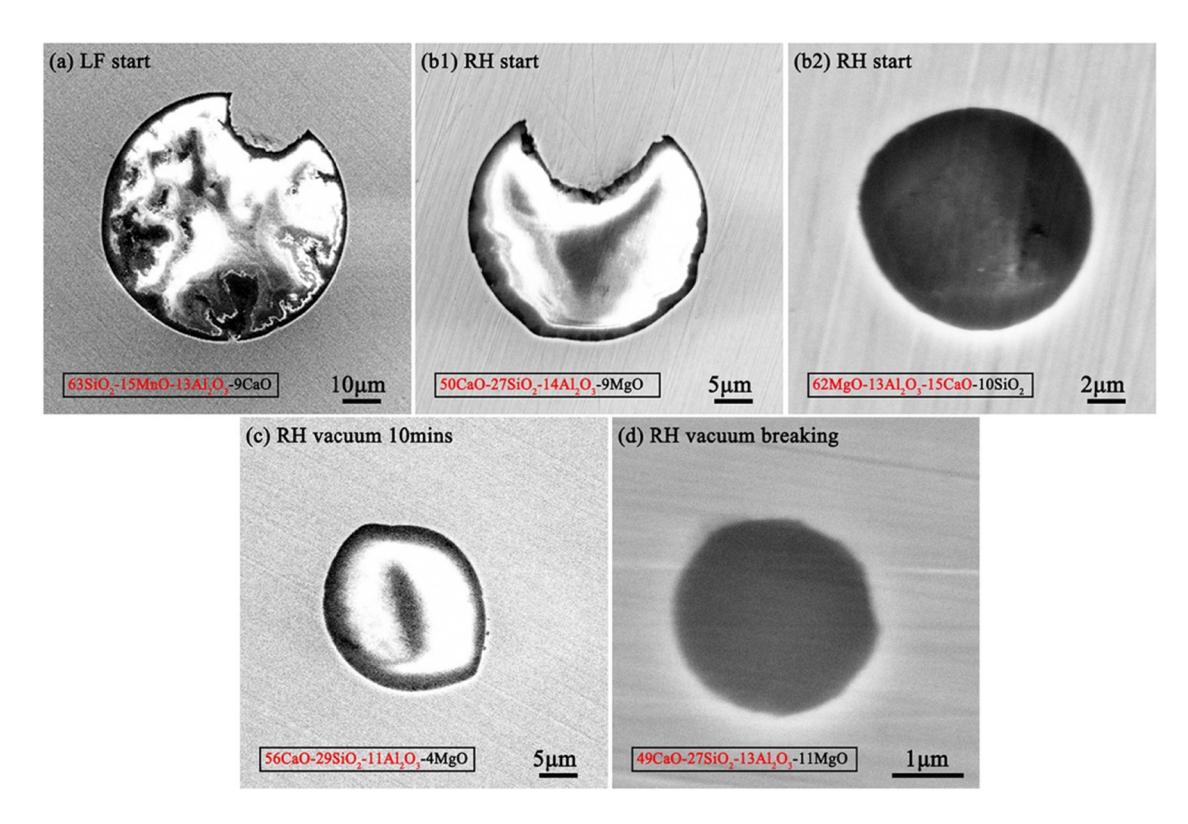


Figure 2: Morphology and chemical composition of typical inclusions during the LF-RH refining process in heavy rail steel: (a) LF start; (b1 and b2) RH start; (c) RH vacuum holding for 10 min; and (d) RH vacuum breaking.

4 — Hongbo Liu et al. DE GRUYTER

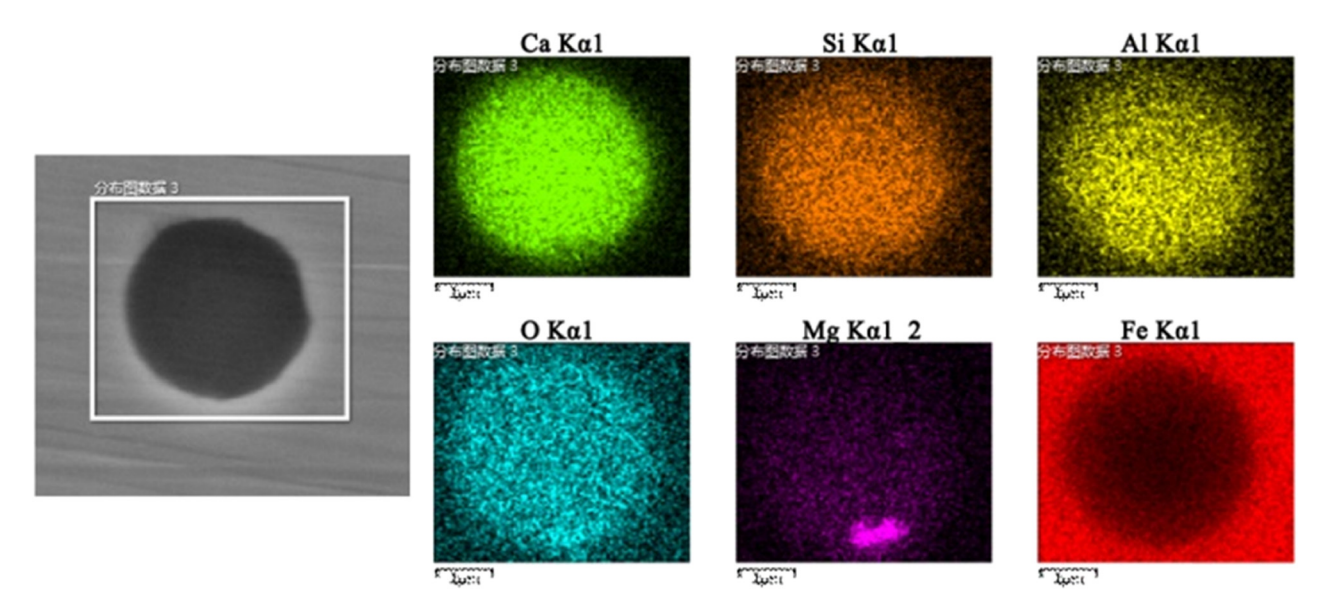


Figure 3: Scanning electron microscopy images and element mappings of the CaO-SiO₂-Al₂O₃-type inclusion formed at the vacuum breaking stage in heavy rail steel.

3.3 Composition evolution of inclusions

Figure 4 shows the composition distribution of inclusions in heavy rail steel. The blue dotted line, green the dotted line and the red solid line represent the liquids at 1,600, 1,500 and 1,400°C, respectively. The variation trends of the average composition of inclusions are given in Figure 5. The composition evolutions of inclusions in heavy rail steel at different stages of the LF–RH refining process were analyzed.

As shown in Figures 4(a) and 5, there exist MnO-SiO₂-Al₂O₃ and a small amount of CaO-SiO₂-Al₂O₃ system inclusions at LF start. After the converter, a large number of FeMn and FeSi alloys were added to the steel. Therefore, Mn and Si in the alloys react with oxygen in the steel would produce a large number of MnO-SiO₂-Al₂O₃ deoxidation products. After the first-time electrode heating of LF, the MnO-SiO₂-Al₂O₃ inclusions almost disappear and transform into CaO-SiO₂-Al₂O₃ inclusions due to the addition of Ca and Al in added alloys. Meanwhile, there appear CaO-MgO-Al₂O₃ inclusions with a small amount of CaO, which may be caused by the erosion of refractory materials. At the same time, the average composition of inclusions in steel is 3MnO-21CaO-19SiO₂-38Al₂O₃-17MgO. As illustrated in Figure 4(c), with the progress of LF refining, the content of MgO reaches the maximum value of 29% after the second-time electrode heating. The inclusions in steel are mainly CaO-SiO₂-Al₂O₃ and CaO-MgO-Al₂O₃. It can be seen that the average of CaO-SiO₂-Al₂O₃ inclusions is mainly distributed in the liquids with a low melting point,

while the average compositions of CaO-MgO-Al₂O₃ inclusions are distributed in the high melting point region, which is typical of high melting point inclusions. The content of CaO and SiO₂ in the conclusions continued to increase while the content of MgO and Al₂O₃ showed a downward trend in the RH station in Figure 5. At this time, the average composition of the inclusions in the steel is 0.5MnO-34CaO-24- $SiO_2-13Al_2O_3-23MgO$. The number of CaO-MgO-Al₂O₃ inclusions with high melting point decreased dramatically. However, the number of CaO-SiO₂-Al₂O₃ inclusions with low melting point changed little when RH vacuum was maintained for 5 min, indicating that RH vacuum treatment has an obvious removal effect on high melting point inclusions. The reason is that the contact angle between the high melting point inclusions with high MgO and high Al contents at 1,600°C liquid steel is greater than 90° [11–14], such inclusions have poor wettability with liquid steel and can be easily aggregated and grown in the RH vacuum treatment process and finally absorbed by slag. As shown in Figure 4(f), when RH vacuum is maintained for 10 min, the high melting CaO-MgO-Al₂O₃ system inclusions were basically disappeared, while the number of low melting point CaO-SiO₂-Al₂O₃ system inclusions is almost no changes. At this moment, the average composition of inclusions is 0.1MnO-43CaO-30SiO₂-13A l_2O_3 -8MgO. It is noted that the average composition of inclusions remains basically unchanged when the RH vacuum is maintained for 15 min, RH break and RH soft blowing.

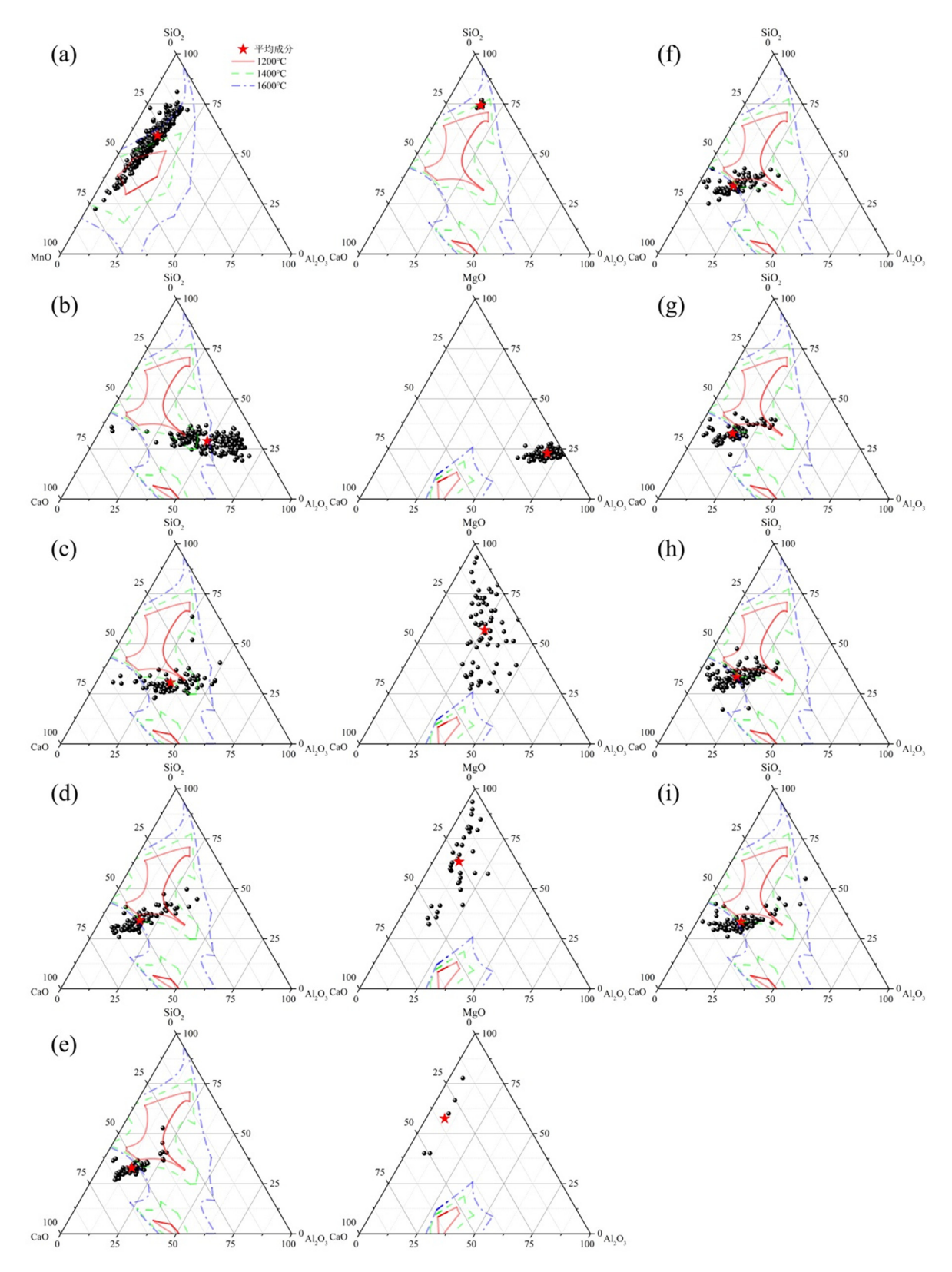


Figure 4: Composition distribution of inclusions at different stages during the LF-RH refining process in heavy rail steel: (a) LF start; (b) after $first-time\ electrode\ heating; (c)\ after\ second-time\ electrode\ heating; (d)\ RH\ start; (e)\ RH\ vacuum\ holding\ for\ 5\ min; (f)\ RH\ vacuum\ holding\ for\ 5\ min; (e)\ RH\ vacuum\ holding\ for\ 5\ min; (f)\ RH\ vacuum\ holding\ for\ 5\ min; ($ 10 min; (g) RH vacuum holding for 15 min; (h) RH vacuum breaking; and (i) after RH soft blowing.

6 — Hongbo Liu et al. DE GRUYTER

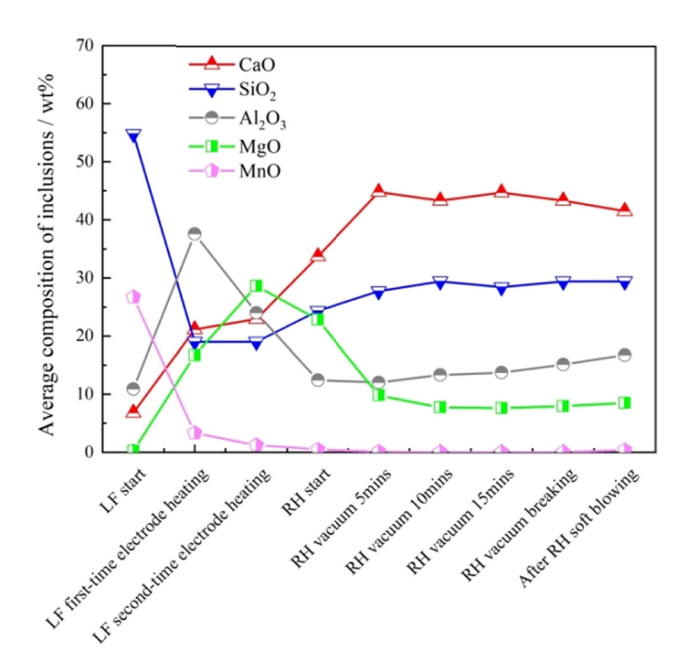


Figure 5: Evolution of the average composition of inclusions during the LF-RH refining process in heavy rail steel.

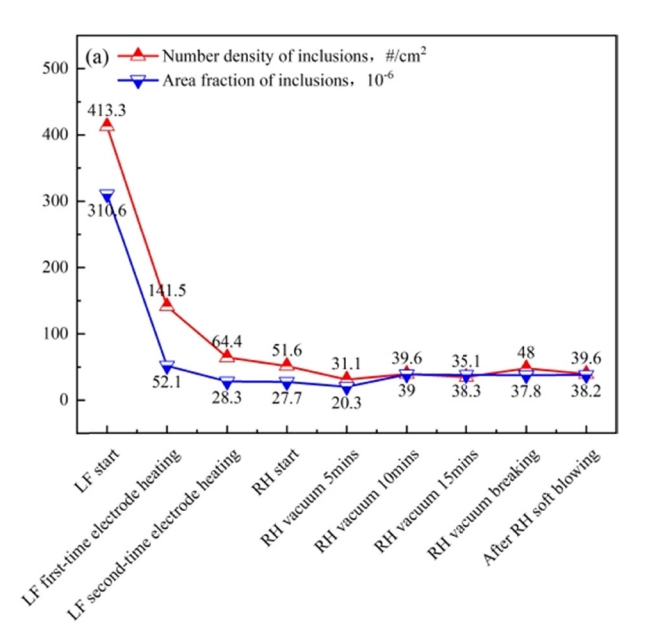
3.4 Variation in inclusions' number density, area fraction and size in steel

The variation in inclusions' number density, area fraction, average length and maximum length in heavy rail steel is demonstrated in Figure 6. It can be seen from Figure 6(a), both the number density and area fraction

of inclusions decrease significantly, indicating that LF-RH refining can obviously remove the inclusions in heavy rail steel. The number density of inclusions was 413.3 cm⁻² at LF start, and then, it decreased sharply to 64.4 cm⁻² after the second-time electrode heating. The number density of inclusions at RH start was 51.6 cm⁻²; subsequently, it reduced to 31.1 cm⁻² after 5 min of RH vacuum treatment, which means that RH vacuum treatment can obviously remove the inclusions in the steel. Afterward, the number density and area fraction change little when the RH vacuum holds for 5-15 min. However, the number density of inclusions increased from 35.1 to 48 cm⁻² at the RH break stage, whereas the area fraction of inclusions has no significant change. After RH soft blowing, the number density of inclusions decreased slightly to 39.6 cm⁻². In addition, Figure 6(b) shows the change in the maximum size and average size of inclusions in steel, the maximum size of inclusions reaches 87 µm while the average size decreases from 9.3 to 5.1 µm when RH vacuum from 5 to 15 min. At RH break, the number density of inclusions increases and the average size increases from 5.1 to 8.1 µm due to the short charging time and a small amount of steel slag mixing.

4 Conclusions

With the LF-RH refining process, the mass fraction of TO in heavy rail steel continues to be decreased, the mass



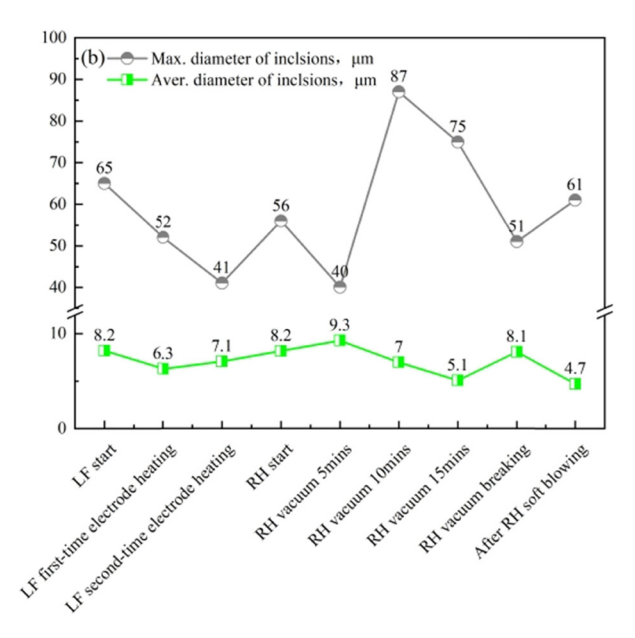


Figure 6: Number density, area fraction, average length and maximum length of inclusions at different stages during the LF-RH refining process in heavy rail steel: (a) number density and area fraction and (b) average and maximum length.

fraction of TO in RH soft-blowing sample is 7×10^{-6} . Meanwhile, the content of N in steel was increased during the LF refining process, which could be effectively removed in the RH vacuum treatment stage, and the mass fraction of N was 33×10^{-6} when RH vacuum hold for 5 min.

The main inclusions at LF start were MnO–SiO $_2$ –Al $_2$ O $_3$, which were manganese-silicon deoxidation products. With the addition of calcium and aluminum in ferroalloy, the MnO–SiO $_2$ –Al $_2$ O $_3$ inclusions were transformed into CaO–SiO $_2$ –Al $_2$ O $_3$ inclusions. The average MgO content in the inclusions reached the highest value of 29% after the second-time electrode-heating stage. At this moment, the inclusions mainly included CaO–SiO $_2$ –Al $_2$ O $_3$ with a low melting point and CaO–MgO–Al $_2$ O $_3$ with a high melting point.

The $\text{CaO-MgO-Al}_2\text{O}_3$ inclusions with the high melting point could be effectively removed by RH vacuum treatment, which were disappeared after RH vacuum maintained for 10 min. However, the average compositions of inclusions had no obvious change from RH vacuum holding for 15 min, RH vacuum break to RH soft blowing.

Acknowledgment: The authors would like to express sincere thanks to Dr. Jie Zhang of the University of Science and Technology Beijing, China, for his careful revision of this article.

Funding information: This study was financially supported by the Natural Science Foundation of Hebei Province (Grant No. E2021318004), the Central Guidance on Local Science and Technology Development Fund of Hebei Province (Grant No. 216Z1009G) and the Open Project Program of Beijing Key Laboratory of Pipeline Critical Technology and Equipment for Deepwater Oil & Gas Development (Grant No. BIPT2019001).

Author contributions: Hongbo Liu: writing the original draft; Rongyuan Xie: writing the original draft, methodology and reviewing the document; Min Li, Zhanli Liu: inclusion analysis; Haibin Yang, Qiang Wang: industry test; and Caidong Zhang, Hongyong Yao, Zhiqiang Tian, Ju Kang: resources.

Conflict of interest: The authors state no conflict of interest.

Data availability statement: All authors can confirm that all data used in this article can be published in High Temperature Materials and Processes.

References

- [1] Yuchang, W. Key technologies of cleanliness and homogeneity control for high-speed heavy rail steel. *China Metallurgy*, Vol. 4, 2015, pp. 7–11.
- [2] Yulei, Z., Z. Chao, H. Xiaoshuai, L. Tian, S. Yanhui, and Z. Min. Effect of sulfur content on non-metallic inclusions of heavy rail steel. *Journal of Iron and Steel Research*, Vol. 34, 2022, pp. 799–806.
- [3] Shuai, Z., L. Xu, P. Ruibao, Y. Hui, and L. Zelin. Control of total content of aluminium in heavy rail steel. *Angang technology*, Vol. 437, 2022, pp. 68–72.
- [4] Garber, A. K., A. M. Arsenkin, K. V. Grigorovich, S. S. Shibaev, A. V. Kushnarev, and Y. P. Petrenko. Analysis of various versions of the deoxidation of rail steel at OAO NTMK. *Russian Metalluray*, Vol. 7, 2009, pp. 581–586.
- [5] Godik, L. A., N. A. Kozyrev, and L. V. Korneva. Optimizing the oxygen content in rail steel. *Steel in Translation*, Vol. 3, 2009, pp. 240–242.
- [6] Lintian, S. Secondary refining and continuous casting of heavy rail steel. *Iron steel and vanadium titanium*, Vol. 2, 1996, pp. 51–57.
- [7] Zhiyong, C., C. Yanping, Y. Wen, X. Guangsheng, L. Nan, and Y. Zhengyuan. Thermodynamics and industrial practice of the formation of non-metallic inclusions during deoxidization of heavy rail steel. *Steel making*, Vol. 4, 2020, pp. 12–18.
- [8] Zhiyong, C., X. Guangsheng, and B. Guojun. Research on Typical Inclusions of Baotou steel Heavy Rail. Science and Technology of Baotou Steel, Vol. 5, 2016, pp. 45–48.
- [9] Jianghua, Q., Z. Jianguo, C. Guangyou, Z. Jianhua, Z. Wanjun, and P. Zhugang. Discussion on sources of large inclusions in heavy rail steel. *Steel making*, Vol. 6, 2017, pp. 62–66.
- [10] Yanping, C., C. Zhiyong, L. Nan, Y. Wen, W. Jujin, and Z. Lifeng. Formation and control of spinel inclusions in high-speed heavy rail steel. *Iron and Steel*, Vol. 55, 2020, pp. 38–46.
- [11] Cramb, A. and I. Jimbo. Interfacial considerations in continuous casting. *Iron Steelmaker*, Vol. 6, 1989, pp. 43–55.
- [12] Kang, Y., B. Sahebkar, P. R. Scheller, K. Morita, and D. Sichen. Observation on physical growth of nonmetallic inclusion in liquid steel during ladle treatment. *Metallurgical and Materials Transactions B*, Vol. 3, 2011, pp. 522–534.
- [13] Nakashima, K. and K. Mori. Interfacial properties of liquid iron alloys and liquid slags relating to iron-and steel-making processes. ISIJ international, Vol. 1, 1992, pp. 11–18.
- [14] Shinozaki N., N. Echida, K. Mukai, Y. Takahashi, and Y. Tanaka. Wettability of Al₂O₃-MgO, ZrO₂-CaO, Al₂O₃-CaO substrates with molten iron. *Tetsu-to-Hagané*, Vol. 10, 1994, pp. 748-753.